Focusing Capability of a Phononic Crystal Based on a Hollow Metallic Structure

Anne-Christine Hladky-Hennion, Charles Croënne, Jérôme O. Vasseur, Lionel Haumesser, and Andrew N. Norris

Abstract—The dispersion curves of a phononic crystal (PC) based on a hollow metallic structure are presented. They exhibit a negative refraction dispersion branch and perfect refractive index matching with the surrounding water, leading to focusing capability. Numerical and experimental results are reported for a flat PC lens. The characteristics of the focal spot (intensity, dimensions, etc.) are numerically and experimentally investigated with the goal of finding the frequency of the optimal imaging performance.

I. Introduction

DHONONIC crystals (PCs) are periodic composite elastic media that have attracted a great deal of interest because they may exhibit unusual acoustic properties which are unavailable in natural materials. Stopbands, i.e., frequency ranges where wave propagation is forbidden, may appear depending upon the constituent materials involved and the geometry of the underlying lattice structure. Applications of this property include frequency filtering and wave guiding. When the band structure exhibits a branch with a negative slope, negative refraction of acoustic waves may occur. This phenomenon has been largely investigated both theoretically and experimentally [1], [2]. In particular, focusing of acoustic waves may be observed when the refractive indices of the PC lens and the surrounding fluid medium are matched. Moreover, depending on the position of the source and on the geometry of the lens, super-resolution i.e., a resolution lower that the diffraction limit can be achieved. This property is due to the presence of bound surface or slab modes which can resonantly couple to the evanescent fields emitted by the source, and thus contribute to image formation [3]–[5], in contrast with classical lenses, where only propagative field components are exploited, leading to the half-wavelength resolution limit. Acoustic super resolution has been dem-

Manuscript received December 12, 2013; accepted May 7, 2014. This research study was supported by the Agence Nationale de la Recherche (ANR) and the Office of Naval Research (ONR). The authors wish to thank the Fédération Acoustique du Nord Ouest (FANO), FR 3110 CNRS, for its financial support in the manufacturing of the device, made in the Blois Institute of Technology, Blois, France.

A.-C. Hladky-Hennion, C. Croënne, and J. O. Vasseur are with the Institut d'Électronique de Microélectronique et de Nanotechnologie (IEMN), UMR CNRS 8520, Lille, France (e-mail: jerome.vasseur@univ-lille1.fr).

L. Haumesser is with the University François Rabelais, Tours, France. A. N. Norris is with Rutgers University, Piscataway, NJ. DOI http://dx.doi.org/10.1109/TUFFC.2014.3038

onstrated with a flat PC lens made of a triangular lattice of steel rods in methanol, surrounded by water [6]. Technological applications of the wave-focusing phenomenon may be considered especially for the rapeutic devices, but this requires the design of a device with a solid matrix that can be easily handled. The possibility of negative refraction and focusing in PCs with an elastic solid as matrix is a difficult topic because of the coexistence of longitudinal and transverse waves. First studies have concerned a PC made of a triangular lattice of steel rods in epoxy. With this device, a branch with a negative slope can be coupled with an acoustic wave in the surrounding fluid, and negative refraction of waves has been demonstrated. Nevertheless, the device was not a good candidate for wave focusing because index matching was not verified [7]. Another original structure proposed by Norris [8] was subsequently investigated. It consists of a honeycomb lattice of aluminum arms with additional masses at the vertices of the hexagons. In the long wavelength limit this structure behaves as water, with mass density and longitudinal velocity close to those of water and a very low shear velocity. Calculated dispersion curves highlight that this metal-water structure (MWS) is a potential candidate for wave focusing because 1) a negative branch crosses the water sound line (i.e., the line showing sound wave dispersion in water), and thus index matching is obtained; 2) the branch with a negative slope corresponds to a mainly longitudinal mode that can be coupled with an external fluid medium; and 3) the equifrequency contours are almost circular, indicating the isotropy of the device. In a recent paper [9], we have shown that the MWS exhibits a negative refraction dispersion branch with a perfect refractive index matching with surrounding water, and focusing capability.

The purpose of the present paper is to further understand the negative index properties of the MWS using both numerical and experimental analyses. The outline of the paper is as follows: In Section II, the structure is defined and the symmetry of the branches in the dispersion curves is investigated to understand the transmission of the wave from the external fluid medium into the PC. In Section III, numerical simulations are used to find the frequency of the optimal imaging performance by quantitative study of the focal spot characteristics (position, peak level, extent in width and in depth) as a function of the frequency. Experiments that confirm the numerical observations are presented in Section IV. Final conclusions are given in Section V.

II. THE PC STRUCTURE, DISPERSION CURVES, AND MODE SYMMETRIES

The MWS is a two-dimensional network of arms, made of aluminum, arranged in a hexagonal lattice (Fig. 1). The structure is supposed to be infinite and uniform along the z-direction. Additional star-shaped masses are placed at the vertices of the lattice to control the effective density of the structure, whereas the effective elasticity is controlled by the thickness of the arms. For the MWS considered here, the width of the interconnecting arms, the width and the length of the star arms, and the sides of the regular hexagon are l = 0.5 mm, l' = 1.51 mm, h = 3.02 mm, and a = 6.445 mm, respectively. Dispersion curves are calculated with the ATILA finite element (FE) code [10], using periodic boundary conditions. The simulated unit cell is presented as a black rhombus in Fig. 1 ($b = a\sqrt{3} =$ 11.16 mm) where only the solid part is meshed. The dispersion curves are presented for the ΓX - and ΓJ -directions on Fig. 2, and branches are split into symmetric and antisymmetric branches with respect to the propagation direction. Full dispersion curves along the ΓXJ path in the first Brillouin zone are presented in [9]. The solid curve, called the sonic line, is the dispersion curve in water. The MWS has characteristics very close to those of water in the quasi-static regime, by design [8]. Indeed it can be seen that at low frequencies the dispersion curve in the MWS follows the sonic line. Additionally, because 37% of the volume is occupied by aluminum, with density 2700 kg/m³, the quasi-static effective density of the MWS is very close to 1000 kg/m³, the density of water. Note the anti-crossing of the two branches with the same symmetry along the ΓJ path at around 10 kHz (see inset of Fig. 2). The dispersion curves for both directions (ΓX and ΓJ) exhibit a branch at higher frequencies with a negative slope that intercepts the sonic line. Index matching between the PC and water is achieved at the intersection point, at which frequency focusing can occur. Fig. 3 presents the corresponding displacement field in the unit cell for the two principal propagation directions.

For propagation in the ΓX direction, the negative branch crossing point is at 71.6 kHz and the corresponding displacement field [Fig. 3(a)] is symmetric with respect to the propagation direction (vertical arrow). The crossing point for propagation in the Γ J-direction is at 70.8 kHz, but we note an important difference in the displacement field map [Fig. 3(b)], which is antisymmetric with respect to the propagation direction (horizontal arrow). In this case, a line integral of the field taken along the direction perpendicular to the propagation direction vanishes, and thus the coupling coefficient with a normally incident plane wave is reduced to zero, leading to the deafband effect [11]. However, for waves normally incident in the Γ X-direction [Fig. 3(a)] the symmetry of the motion in the MWS guarantees coupling with the acoustic waves in the fluid. This motivated our design of the MWS so that normal incidence corresponds to the Γ X-direction. For our

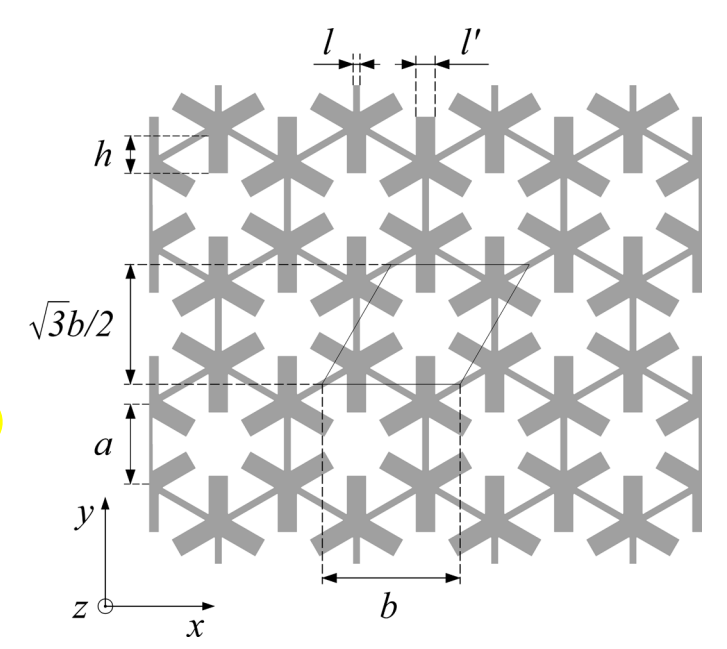


Fig. 1. Description of the MWS and the relevant geometrical parameters. The black rhombus shows one unit cell of the structure.

MWS lens, the deaf propagation direction does not correspond to the surface normal, and based on this crystal orientation choice, we can expect a significant contribution from obliquely incident acoustic waves to the overall transmission in the focusing experiment.

When the phase velocities in the PC and the external water medium match for any angle of incidence, the equifrequency contours (EFCs) are circular and the structure is isotropic. In the case of the MWS, the EFCs (see [9] for details) are almost, but not quite, circular because of slightly different intersection points between the negative

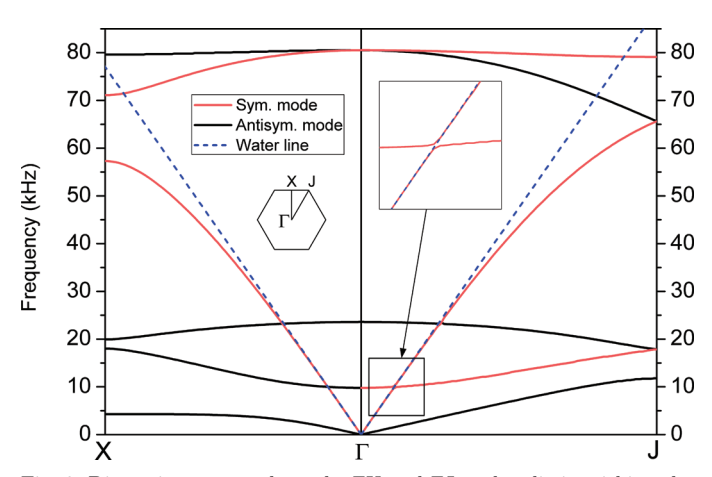


Fig. 2. Dispersion curves along the ΓX and ΓJ paths, distinguishing the symmetric and antisymmetric modes with respect to the propagation direction. The dashed line is the sonic line in water. One inset shows a zoomed-in view of the anti-crossing of two symmetric branches along the ΓJ path. The other inset represents the first Brillouin zone with its high symmetry points. Note that ΓX corresponds to waves propagating along the y-direction in real space.

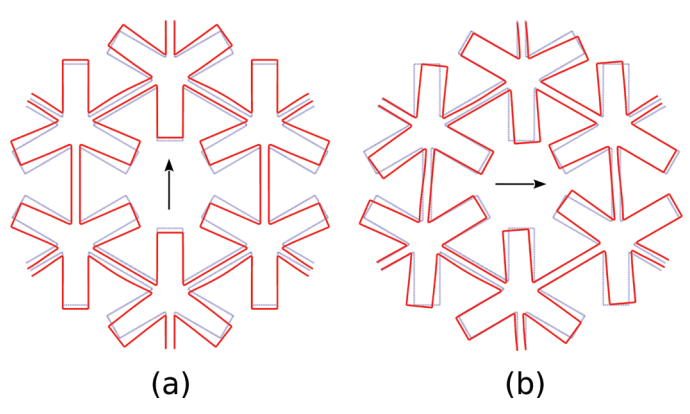


Fig. 3. Displacement field maps at the intersection point between the dispersion branch with negative slope and the sonic line on the (a) ΓX and (b) ΓJ paths. Dashed blue lines correspond to the rest position. The arrow indicates the propagation direction.

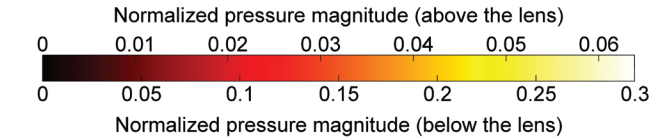
branch and the sonic line along the principal propagation directions (71.6 kHz along the ΓX path, 70.8 kHz along the ΓJ path). This results in a small amount of anisotropy for the acoustic wave propagation through the MWS.

In summary, the crossing of the sonic line with the negative branch ensures that the crucial all-angle negative refraction criterion is satisfied [12]. At the same time, the symmetry of each branch with respect to the propagation direction plays a critical role in the transmission of the wave through the lens. For these reasons, and based on the numerical experiments, the lens is built with the MWS oriented in the Γ X-direction to get the best transmission through the lens, by coupling of the waterborne acoustic wave to the branch with negative slope in the MWS. Therefore, the best focusing is expected with this design at 71.6 kHz, the intersection point in the Γ X-direction.

III. NUMERICAL ANALYSIS OF THE FOCUSING EFFECT

Numerical calculations are performed to demonstrate the focusing capability of the MWS over an extended frequency range within the branch with a negative slope. The lens considered is 6 cells thick and 32 cells wide and surrounded by water; see Fig. 4. Harmonic simulations are performed using the finite element code ATILA [9]. A point source emitting cylindrical waves at 71.6 kHz is positioned before the slab (at position y_0), 8.9 mm away from the lens. Because this distance only corresponds to about 0.4 wavelength, the evanescent field emitted by the point source (and carrying information about its subwavelength size) will easily reach the slab interface and possibly excite resonant modes in the lens, which are of key importance in the super-resolution effect. The focusing effect is clearly observed (Fig. 4).

Performance of the MWS slab as an imaging device can be assessed from the characteristics of the focal spot, specifically: position (y_m) , peak level, and extent in width (along x) and depth (along y). The distance between the point source and the focal spot center is equal to 119.3 mm.



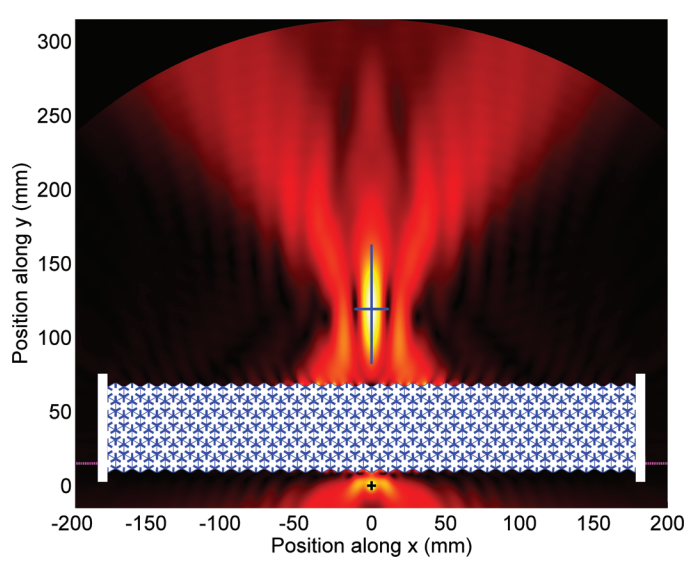


Fig. 4. Simulated pressure magnitude field map at 71.6 kHz normalized to source level of 1. The MWS structure is shown in blue, and the air/unmeshed regions in white. The source is located below the slab at the center of the black cross [i.e., at (x,y) = (0,0)], and the focusing effect is observed above. For clarity, a different color scale is used below the slab (below the dotted magenta line). The horizontal and vertical blue lines at the focal spot show its measured width and depth (lateral resolution and axial FWHM).

For a classical negative index lens, we expect this distance to be constant and equal to twice the slab thickness d [13]. In the MWS case, the effective thickness of the slab is not immediately obvious because the interfaces are not flat. However, if we consider that we have 6 rows of hexagonal cells with a separation of $\sqrt{3}b/2$ (see Fig. 1), we obtain d = 58 mm, and about 2.06d for the source-image distance at 71.6 kHz, in good agreement with theory. The peak amplitude is much smaller than the source amplitude, with a pressure ratio close to 6.4% because of a significant impedance mismatch between water and MWS far from the quasi-static regime. The extent of the focal spot in depth can be measured using the full-width at half-maximum (FWHM) of the pressure magnitude probed along a line perpendicular to the lens passing through the focal spot, and is equal to about 80.4 mm (3.87 wavelengths). Lateral extent of the focal spot could also be measured using a FWHM, but to obtain the actual lateral resolution of the system as defined by the Rayleigh criterion, the main peak of the pressure magnitude is probed along a line parallel to the lens passing through the focal spot and then fit to a cardinal sine function [6]. The half-width of the main lobe of the fitted function then corresponds to the actual resolution. It is found to be 11.58 mm, i.e., about 0.56 wavelength, which is slightly larger than the resolution limit of half the wavelength.

It should be noted that the 71.6 kHz operation frequency has been selected based upon the band diagram for the infinite MWS. In other words, we assumed that the EFC is the critical parameter to find the frequency of optimal imaging performance. To verify this assumption, the same harmonic FE simulation is performed for frequencies ranging from 68.8 to 74.8 kHz, with a 0.2 kHz frequency step. The variations of the four focal spot characteristics (position, peak level, and extents in width and in depth) defined previously are shown in Fig. 5 as a function of frequency. Additionally, Fig. 6 presents the pressure magnitudes probed along the lines passing through the focal spot (a) perpendicular and (b) parallel to the lens for all frequencies considered, as images with the horizontal and vertical axes indicating the spatial location and frequency, respectively.

We note from Figs. 5(a) and 6(a) that the source-image distance increases with frequency. This trend is consistent with the approximate formula d(1 + 1/|n|) [14] because the (negative) effective index n is increasing with frequency in the range under study [9]. As already stated, at 71.6 kHz, the theoretical prediction for the spot location is almost satisfied $((y_m - y_0)/d = 2.06)$, but the frequency sweep shows that matching would be improved with the operation frequency decreased to 71.2 kHz $((y_m - y_0)/d =$ 2). On the contrary, Fig. 5(c) indicates that operation frequency should be increased to about 72.8 kHz if we want to maximize the amplitude of the focal spot, with a maximum pressure ratio close to 7.2%. A minimum lateral size of the focal spot could be expected at 71.6 kHz. Indeed, in an ideal negative index flat lens, contributions from the evanescent and propagative wave components are balanced so that the optimal lateral resolution is achieved in the $(y_m - y_0)/d = 2$ plane when the index is equal to -1 [3], [13], but this property is not necessarily present in actual photonic [4] or phononic crystals with negative indices. The frequency variations described here show that the MWS does not possess this property. In fact, better resolutions are achieved at lower frequencies, when the index matching condition is no longer respected. This effect could be attributed in part to the variation of the focal spot position; because it gets closer to the lens at lower frequencies, a more significant contribution from the evanescent fields related to the slab resonant modes can be expected. Additionally, a discontinuity in the frequency evolution of $(y_m - y_0)/d$ can be noted at 68.8 kHz. It arises from the appearance of a secondary spot very close to the slab at lower frequencies. Fig. 6(a) shows that this spot is already present around 70 kHz, but it only becomes brighter than the main focal spot around 68.8 kHz. Again, this shows that we are leaving the frequency region where the ideal (n = -1) negative index flat lens concept is relevant, and are transitioning to a system in which the evanescent wave components at the slab output interface become an important factor [4]. Note that in all cases, the calculated resolution is above the theoretical limit of 3a/4[see the solid line in Figs. 5(g) and 5(h)] which can be de-

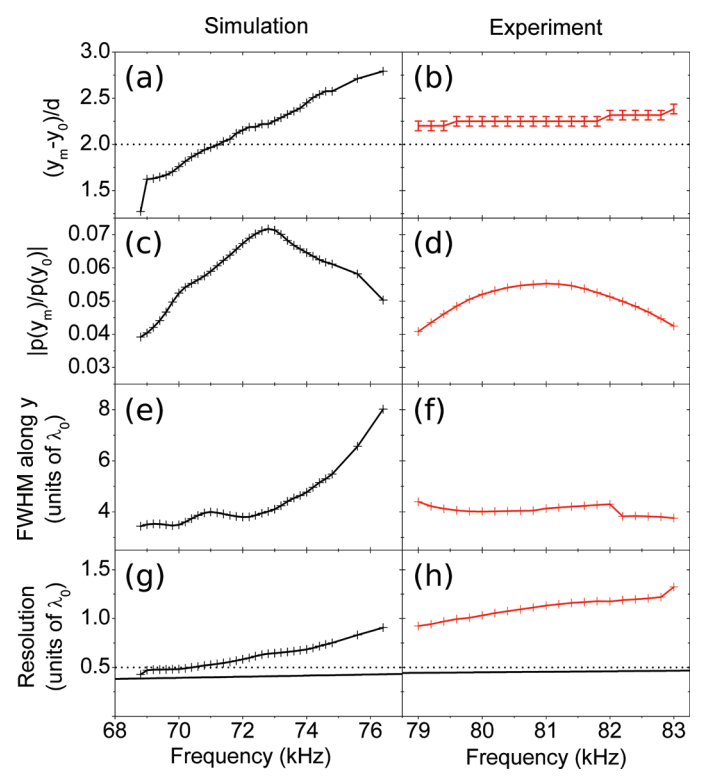


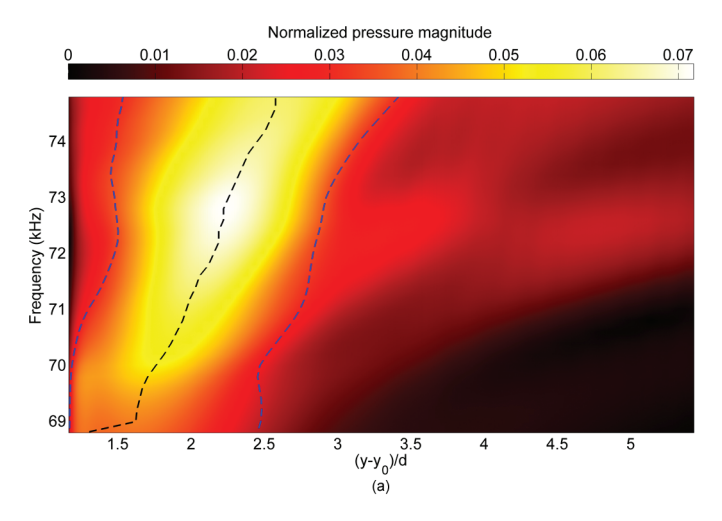
Fig. 5. [(a), (c), (e), and (g)] Simulated and [(b), (d), (f), and (h)] experimental frequency dependence of the four focal spot characteristics [(a) and (b) position; (c) and (d) peak level; and (e) and (f) extent in width and (g) and (h) in depth]. The horizontal dashed line in (a) and (b) shows the theoretical position of the spot for a classical negative index lens, whereas the horizontal dashed line in (g) and (h) indicates the conventional $\lambda_0/2$ resolution limit. Additionally, the solid line with no marker indicates the theoretical resolution limit of 3a/4 (in units of wavelength).

duced if we assume unit transmission for all waves (both propagative and evanescent) with a transverse wavevector component inside the first Brillouin zone [15]. In summary, even though the FE MWS slab simulations show that reasonable performance can be obtained at the frequency predicted by the band diagram study (i.e., 71.6 kHz), the optimal choice will depend on the importance given to the individual performance criteria.

IV. EXPERIMENTAL RESULTS ON THE FOCUSING OF THE MWS LENS

Experiments are performed using a sample made of fifteen 5-mm-thick aluminum plates stuck together. A water jet process is used to cut each plate following the geometry described previously (Fig. 7). The first and last plates are plain aluminum plates. The whole sample is 75 mm high, 265 mm wide, and its thickness varies between 58.1 mm and 60 mm, because the shape of the interface is not flat.

The diagram of the experimental arrangement is shown in Fig. 8. The source is the focal spot of a spherically focused transducer, with a 12.7 mm diameter and



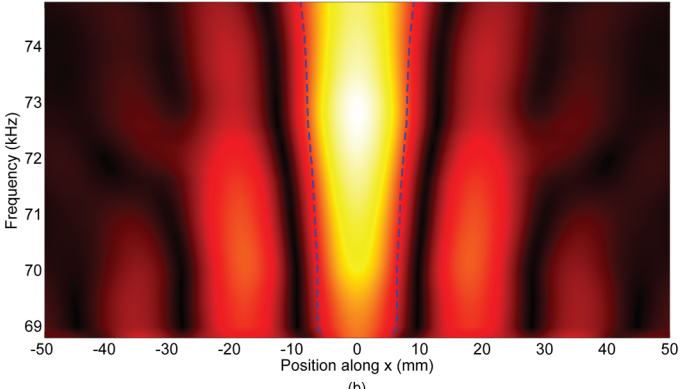


Fig. 6. Simulated normalized pressure magnitude field maps on individual lines, as a function of frequency. Horizontal and vertical axes represent the spatial location and the frequency, respectively. In (a) and (b), the lines perpendicular and parallel, respectively, to the slab interfaces passing through the focal spot are considered. The spatial axis in (a) is normalized to allow direct comparison with the theoretical position $(y_m - y_0 = 2d)$. The dashed black line in (a) shows the position of the maximum; in (b) it is always located at x = 0. The dashed blue lines indicate the measured sizes of the focal spot along the axial and lateral directions (see the two blue lines on Fig. 4).

a 30.48 mm focal length. The 1-Vpp electrical excitation containing 3 periods of sine at 75 kHz and delivered by a waveform generator is applied to a +55 dB amplifier. The signal obtained is fed into the emitter transducer. The receiver transducer is unfocused, with the same diameter as the emitter. Note that the size of the transducers is close to the wavelength. This will limit the precision of the lateral resolution measurement because the expected values are lower than the wavelength. The design of transducers with sub-wavelength dimensions remains a challenging task and is beyond the scope of this paper. The free-field characteristics of the source are measured in a 69×60 mm rectangular area (delimited with a solid line in Fig. 8) using a planar receiver transducer having the same diameter as the emitter. The measurement grid starts 1 mm away from the radiating spherical cap of the transducer. The linear displacement intervals are 3 mm each, corresponding to 0.16 and 0.17 wavelength at 79 kHz and 84 kHz,

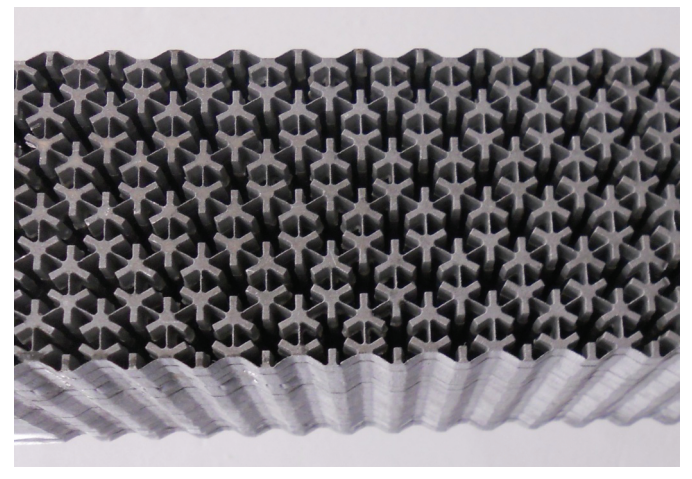


Fig. 7. Photograph of the MWS phononic crystal with end cap plates removed.

respectively. Measurements are performed in a water tank whose size allows us to distinguish between the wall echo signals and the useful signal components in the time-domain recordings. Furthermore, waves reflected from the receiver are filtered out to keep waves from the source only. Signals collected from the image area are processed in the same way when the MWS is present. The waves refracted by the MWS are measured on a broader area: 140 \times 144 mm (dashed line frame in Fig. 8), at 4 mm intervals (approximately 1/5 wavelength at 81 kHz).

Fig. 9 presents the evolution of the pressure field around the source (without the lens) and around the focal point (with the lens) in the frequency range corresponding to the narrowest obtained images. It shows the spreading of the focal spot as a function of the frequency. The best focal images are obtained between 80 and 82 kHz. This frequency range is much higher than the expected frequency (71.6 kHz) because of a water leak inside the MWS during the experiment. Numerical calculations for a water-filled MWS have shown that the dispersion curves are shifted toward higher frequencies in this case. More precisely, for

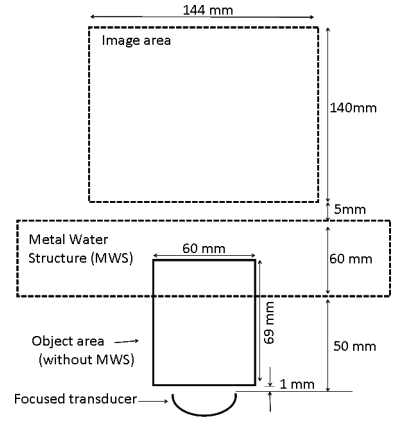
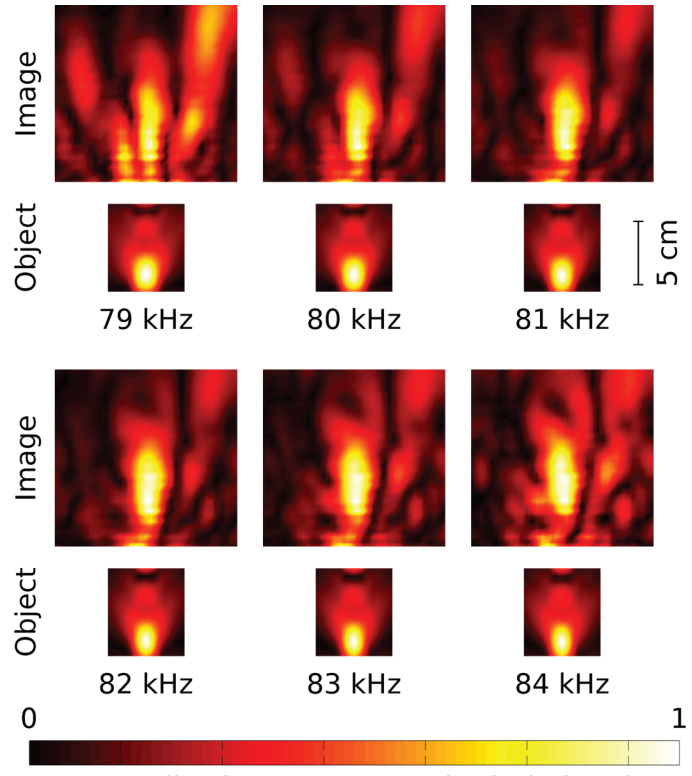


Fig. 8. Dimensional characteristics of the experimental setup (not to scale).



Normalized pressure magnitude (arb. u.)

Fig. 9. Evolution of the measured pressure fields as a function of frequency, from 79 to 84 kHz, both around the source without lens and around the image with the MWS. The measurement areas are as defined in Fig. 8, and the scale shown at the top right is valid for all maps. Amplitude is normalized to the maximum value in each picture.

a fully filled MWS, the lower frequency limit of the negative refraction branch exceeds 83 kHz and consequently there is no crossing with the water sound line in the first Brillouin zone. In fact, the experimental frequency shift seems consistent if we assume an intermediate case with a partially water-filled sample.

Pressure field profile variations are extracted from the data and are displayed as a function of frequency in the 79 to 83 kHz frequency range. Below and above this frequency range, the pressure field around the focal image is highly disturbed. Experimental characteristics of the focal spot of the MWS slab are compared with numerical ones on Fig. 5, in terms of its position (y_m) , its peak level, and its extent in width (along x) and depth (along y).

The experimental distance between the source and the image [Fig. 5(b)] is slightly larger than what would be expected, based upon the numerical results. The vertical error bars correspond to the spatial increment used to scan the image area in the y-direction. Numerical and experimental distances between source and image agree well because their difference is within the range of uncertainty. From 79 to 83 kHz, the distance between the source and the image increases continuously. However, looking carefully at the measurements, a stepwise variation can be noted. This feature is not present in the simulations and

is artificially introduced in the experiments by the 4-mm gap (approximately 1/5 wavelength at 81 kHz) between two successive measurement points.

We note that numerical and experimental variations of the amplitude of the focal spot are similar [Figs. 5(c) and 5(d)]. At the maximum, the amplitude at the focal spot (5%) is of the same order of magnitude as the numerical value for the maximum pressure ratio (7.2%). Comparison of these two values is not straightforward. In the imaging experiments, because we are using the focal spot of a spherically focused transducer with an angular aperture of about 100° at 81 kHz, we can expect that a significant part of the acoustic energy will propagate in out-of-plane directions. Because there is no lattice periodicity along the vertical direction, the effective index along this direction cannot be negative, and thus this energy cannot be focused back into the middle plane. In other words, the image spot will be vertically elongated with respect to the object spot [16], and the fields measured in the middle plane will consequently be lower than expected. However, there is also a competing effect resulting from the finite aperture of the source in the x-y plane which prevents the loss of energy related to the finite width of the lens. The pressure amplitude value measured at the focal spot is affected by these two competing effects, and thus any direct comparison with the values obtained in the 2-D simulations is difficult. Additionally, in the frequency range of interest, the source transverse resolution and FWHM are equal to 1 and 1.6 wavelength (mean values), respectively. It is clear that the characteristics of the source are not suitable to investigate the high-resolution imaging properties of the MWS. Nevertheless, the comparison with the data obtained from the image gives original insight into the focusing capabilities of the MWS. One can observe that experimental and numerical results for the FWHM along y are very similar [Figs. 5(e) and 5(f)]. Moreover, even if the experimental lateral resolution is larger than the numerical one because of the width of the experimental source, the variations as a function of frequency are identical in both cases [Figs. 5(g) and 5(h)]. In fact, experimentally, the lateral resolution is measured by the FWHM. Numerically, a fit of the main peak of the pressure magnitude probed along a line parallel to the lens passing through the focal spot on a cardinal sine function is performed. The different form of the measurement method for the lateral resolution contributes to a 20% difference between numerical and experimental results. Finally, because of the size of the source and the distance between two successive measurement points, better experimental lateral resolution cannot be expected for this configuration.

V. Conclusions

Combined numerical and experimental results have been presented which provide further understanding of the mechanisms underlying the extraordinary focusing property of the MWS. The negative refraction and focusing applications are a consequence of the dispersion curve of the structure, which displays a negative branch that intercepts the sonic line. The modal symmetries of the dispersion curves have been analyzed, indicating preferential coupling of the wave coming from water to the branch with negative slope in the MWS for a certain crystal orientation. This anisotropic feature contrasts with the nearisotropy of the equifrequency contours.

Numerical calculations are performed on a MWS lens, clearly showing the focusing capability of the device. The characteristics of the focal spot are detailed in terms of its position, its peak level, and its extent in width and depth, as a function of the frequency. They show that even if good performance can be obtained at the frequency predicted by the band diagram study (the intersection point between the sonic line and the negative branch), the optimal choice will depend on the importance given to the individual performance criteria. Experiments have been performed on a lens and have shown experimental characteristics in good agreement with the numerical results, even though the experimental source is much larger than the numerical point source. Further studies will include experimental studies with a narrower source, to verify whether super-resolution can be reached with the present MWS design. Additionally, numerical studies will be conducted to search for geometric optimizations that may improve the performance in resolution. These numerical studies will be based in particular on an analysis of the slab resonant modes, which have a key role in the superresolution effect.

References

- [1] P. A. Deymier, Ed., Acoustic Metamaterials and Phononic Crystals (Springer Series in Solid-State Sciences 173), Berlin, Germany: Springer, 2013.
- [2] R. V. Craster and S. Guenneau, Eds., Acoustic Metamaterials (Springer Series in Materials Science 166), Berlin, Germany: Springer, 2013.
- [3] J. B. Pendry, "Negative refraction makes a perfect lens," Phys. Rev. Lett., vol. 85, no. 18, pp. 3966–3969, 2000.
- [4] C. Luo, S. G. Johnson, J. D. Joannopoulos, and J. B. Pendry, "Sub-wavelength imaging in photonic crystals," *Phys. Rev. B*, vol. 68, no. 4, art. no. 045115, 2003.
- [5] X. Zhang and Z. Liu, "Superlenses to overcome the diffraction limit," Nat. Mater., vol. 7, no. 6, pp. 435–441, 2008.
- [6] A. Sukhovich, B. Merheb, K. Muralidharan, J. O. Vasseur, Y. Pennec, P. A. Deymier, and J. H. Page, "Experimental and theoretical evidence for subwavelength imaging in phononic crystals," *Phys. Rev. Lett.*, vol. 102, no. 15, art. no. 154301, 2009.
- [7] C. Croënne, D. Manga, B. Morvan, A. Tinel, B. Dubus, J. Vasseur, and A.-C. Hladky-Hennion, "Negative refraction of longitudinal waves in a two-dimensional solid-solid phononic crystal," *Phys. Rev. B*, vol. 83, no. 5, art. no. 054301, 2011.
- [8] A. N. Norris and A. J. Nagy, "Metal water: A metamaterial for acoustic cloaking," in *Proc. 1st Int. Conf. on Phononic Crystals*, Metamaterials and Optomechanics, 2011, pp. 112–113.
- [9] A.-C. Hladky-Hennion, J. O. Vasseur, G. Haw, C. Croënne, L. Haumesser, and A. N. Norris, "Negative refraction of acoustic waves

- using a foam-like metallic structure," *Appl. Phys. Lett.*, vol. 102, no. 14, art. no. 144103, 2013.
- [10] ATILA, Finite-Element Software Package for the analysis of 2D & 3D structures based on smart materials. Version 6.0.2 User's Manual: November 2010.
- [11] F.-L. Hsiao, A. Khelif, H. Moubchir, A. Choujaa, C.-C. Chen, and V. Laude, "Complete band gaps and deaf bands of triangular and honeycomb water-steel phononic crystals," *J. Appl. Phys.*, vol. 101, no. 4, art. no. 044903, 2007.
- [12] A. Sukhovich, L. Jing, and J. H. Page, "Negative refraction and focusing of ultrasound in 2D phononic crystals," *Phys. Rev. B*, vol. 77, no. 1, art. no. 014301, 2008.
- [13] V. G. Veselago, "The electrodynamics of substances with simultaneously negative values of ε and μ ," Sov. Phys. Usp., vol. 10, no. 4, pp. 509–514, 1968.
- [14] C. Qiu, X. Zhang, and Z. Liu, "Far-field imaging of acoustic waves by a two-dimensional sonic crystal," *Phys. Rev. B*, vol. 71, no. 5, art. no. 054302, 2005.
- [15] J.-F. Robillard, J. Bucay, P. A. Deymier, A. Shelke, K. Muralidharan, B. Merheb, J. O. Vasseur, A. Sukhovich, and J. H. Page, "Resolution limit of a phononic crystal superlens," *Phys. Rev. B*, vol. 83, no. 22, art. no. 224301, 2011.
- [16] M. Ke, Z. Liu, C. Qiu, W. Wang, J. Shi, W. Wen, and P. Sheng, "Negative-refraction imaging with two-dimensional phononic crystals," *Phys. Rev. B*, vol. 72, no. 6, art. no. 064306, 2005.



Anne-Christine Hladky-Hennion was born in Lille, France, in 1965. She was awarded the diplôme d'ingénieur (five-year engineering degree) by the Institut Supérieur de l'Électronique et du Numérique in 1987, and the Ph.D degree in materials science by the Université des Sciences et Technologies de Lille in 1990. She is currently a principal scientist at the CNRS. Her main research interest is the study of phononic structures and metamaterials, using the finite element method, and piezoelectric devices for high-frequency applications. She is a member of the French Acoustical Society (SFA).



Charles Croënne was born in Arras, France, in 1983. He received the engineer degree from the École Centrale de Lille in 2006 and the Ph.D. degree from the Université des Sciences et Technologies de Lille in 2009. After post-doc positions in Lille, at the University of Manitoba (Canada), and at the City University of Hong Kong, he joined the CNRS in 2014 as a junior scientist (CR2). His main research interest is the modeling of periodic structures and metamaterials in the electromagnetic and acoustic domains, and their use in transformation devices (cloaks, hyperlenses, etc.).



Jérôme O. Vasseur was born in Lille, France, in 1965. He obtained a Ph.D. degree in materials science in 1993 and a habilitation thesis in physics in 2002 from the Université des Sciences et Technologies de Lille. He is currently a professor of physics at the Ecole Supérieure du Professorat et de l'Education—Lille Nord de France and a researcher at the Institut d'Electronique, de Microélectronique et de Nanotechnologie. His research activities focus mainly on the modeling of devices based on phononic crystals and metamaterials and their technological applications.



Lionel Haumesser was born in Nantes, France, in 1973. He received the Ph.D. degree in acoustics in 2001 from the University of Le Havre, France. Since 2002, he has been Assistant Professor of applied physics and electronics at the University Francois-Rabelais Institute of Technology of Blois, France. His research activities are in the field of ultrasonics and mainly concern the development of measurement methods for the characterization of passive and piezoelectric-based materials and devices.



Andrew N. Norris received the B.Sc. and M.Sc. degrees in 1977 and 1978, both in mathematical physics from University College Dublin, Ireland, and the Ph.D. degree in applied mathematics and engineering science in 1981 from Northwestern University, Evanston, IL. After postdoctoral positions at Northwestern University and at Exxon Research and Engineering Corporate Laboratories, NJ, he joined Rutgers University, where he is currently Distinguished Professor of Mechanical and Aerospace Engineering in the School of Engi-

neering. Dr. Norris' research involves modeling of acoustic and elastic wave phenomena. His current interests are in developing fundamental mechanical models for metamaterials that exhibit extraordinary wave-bearing properties. He has authored or co-authored more than 150 papers in refereed journals.